Semiclassical decay of topological defects

Szabolcs Borsanyi* and Mark Hindmarsh†
Department of Physics & Astronomy, University of Sussex, Brighton BN1 9QH, UK

Perturbative estimates suggest that extended topological defects such as cosmic strings emit few particles, but numerical simulations of the fields from which they are constructed suggest the opposite. In this paper we study the decay of the two-dimensional prototype of strings, domain walls in a simple scalar theory, solving the underlying quantum field theory in the Hartree approximation. We conclude that including the quantum effects makes the picture clear: the defects do not directly transform into particles, but there is a non-perturbative channel to microscopic classical structures in the form of propagating waves and persistent localised oscillations, which operates over a huge separation of scales. When quantum effects are included, the microscopic classical structures can decay into particles.

PACS numbers: 03.65.Pm, 11.10.-z, 11.27.+d
Keywords: Domain walls; Cosmic strings; Oscillons; Hartree approximation

I. INTRODUCTION

Our current fundamental theory of the universe suggests higher order symmetries which are successively broken as the universe cools. This naturally leads to the formation of topological defect networks [1]. Such extended objects could play a role in the early formation of structure in the universe [2, 3, 4]. Indeed, recent calculations [5] show that models with cosmic strings and other topological defects fit the Cosmic Microwave Background data better than the standard power-law ΛCDM model.

Analytical estimates suggest that particle production from decaying strings (or, in two dimensions: domain walls) is suppressed by the separation of cosmological (ℓ) and microscopic (M) scales. The former is the curvature scale of the string, assumed to be of order the Hubble radius, and the latter is determined by the underlying particle physics, typically on the GUT scale. Particle production would mean transforming the energy in the deep infrared into ultraviolet excitations, over something like 58 orders of magnitude in momentum scale. If the cosmic string network is prohibited from losing energy, its dynamics follows the Nambu-Goto action [3, 6]. Perturbation theory suggest that the radiative energy loss is $\sim M/\ell$ [7]. With more insight into the non-linear domain wall dynamics one discovers another channel through cusp annihilation [8], at a rate of $\sim M^{5/3}\ell^{-1/3}$. Once one takes into account the gravitational channel a simple estimate gives $\sim 10^2 M^4/M_p^2$, where M_p is the Plack mass [9], which therefore seems to be dominant for sufficiently large ℓ.

Numerical analysis of the Nambu-Goto action confirms [10, 11, 12] the analytical scaling assumption [13] that implies a string density M/t^{d-1} (in $d = 2, 3$ space dimensions), at least for strings as long as the horizon size. An exact Minkowski space simulation of a string network reveals that fragmentation to loops is the dominant decay process [14, 15], which proceeds down to the smallest scale on the network, which may even be the microscopic scale of the string width [16]. Simulations in an expanding universe [11, 12] broadly confirm this picture, although indicate that the relevant small scale is the initial correlation length [17, 18, 19][52]

However, for strings which are topological defects, we can check this picture by solving the underlying field theory in the classical approximation. This means in practice to integrate the non-linear wave equations on a spatial lattice and to average over an initial ensemble. This approach offers a full insight into all non-perturbative phenomena, although it may be difficult to justify the omission of quantum effects at the microscopic scale. Nevertheless, this method has been successfully used elsewhere, e.g. to explore the dynamics of symmetry breaking [20], or of non-thermal phase transitions [21] in the post-inflationary Universe.

The scaling behaviour suggested by Nambu-Goto simulations is manifest in the classical field dynamics, even though only the microscopic scale appears in the equation of motion. It has been demonstrated in the context of gauge strings in the Abelian Higgs model [22, 23] global strings [23, 24], non-Abelian global strings with junctions [25], and semilocal strings [26, 27], as well as domain walls [28, 29], including models with junctions [30]. The scaling is present in Minkowski as well as expanding space time, and in two as well as three dimensions. It seems to be a universal feature of classical field theories with extended structures.

For strings, a major difference between the numerical solutions of the classical field dynamics and Nambu-Goto simulations is that defects decay into classical radiation [22], at a much faster rate than anticipated from perturbation theory and cusp annihilation. One typically observes a length of string ℓ in a volume ℓ^d, and hence that the string length density is Ł $\sim \ell^{1-d}$. Given a mass per unit length of $\mu \sim M^2$, the energy density in string is $M^2\ell^{1-d}$. Since scaling implies $\ell \sim t$, the energy loss rate per unit length M^2/ℓ. Hence, for a loop of size ℓ, the

*Electronic address: s.borsanyi@sussex.ac.uk
†Electronic address: m.b.hindmarsh@sussex.ac.uk

average energy loss rate is M^2, which is, in fact, greater than the gravitational estimate.

We discover then that the classical scaling implies a strong radiative decay. This is very puzzling in view of the scale separation between the ℓ and M which grows as the simulation proceeds. However, apart from confirming the scaling over more than three orders of magnitude, it is not our purpose to address this important question. Instead we note that up to now it has been unclear if the classical approach is valid here, where dynamics is driven by an interplay between macroscopic and microscopic scales. A check for quantum corrections is crucial.

An alternative to the classical approach is the two-particle-irreducible (2PI) effective action technique, which is based on a selective resummation of perturbative diagrams [31]. Preheating dynamics with non-perturbative particle production [32] and particle thermalisation by scattering [33] are within the range of its applicability. The so far used homogeneous version of this elaborate technique is, however, incapable of addressing the question of defect formation [34].

We can combine these techniques, using the classical approach to form defects and then studying their evolution in the 2PI framework. If we keep the next-to-leading order diagrams in the 2PI effective action, we will gain insight into the scattering and thermalisation of the produced particles. The inhomogeneous variant of the 2PI equations, however, is technically hardly feasible. Keeping the lowest order 2PI diagram yields an approximation scheme, that is equivalent to the well-known Hartree approximation [35, 36]. While scattering between the produced particles is not included here, even the homogeneous version of this scheme could account for the non-perturbatively rapid particle production in the early Universe [37, 38]. The extension of the equations to inhomogeneous backgrounds was historically motivated by the hope that the background field could mediate interaction between the freely streaming particles. Although numerics have shown that the opposite was true [39, 40, 41], this method can be still used for finding the leading quantum corrections to the evolution of classical structures, as has been suggested by a one-dimensional analysis of moving kings [42].

In this paper we analyse the classical solution of the $\lambda\Phi^4$ theory in two space dimensions corrected by the Hartree approximation. In the broken phase this toy model features domain walls, which resemble strings in this low dimensional setting. We check if there is a significant alteration to the kink dynamics by the inclusion of this type of quantum correction.

First we recall the results from classical simulations and demonstrate the scaling behaviour also found in Ref. [28]. Then in section III we introduce the Hartree approximation of the considered model. Next, in section IV we numerically compute the domain wall evolution both in the classical and in the Hartree approximated framework. We discuss possible interpretations of the results in section V, and finally conclude in section VI.

II. CLASSICAL DECAY OF DOMAIN WALLS

A. Model details

The Lagrangian density of our scalar theory is as simple as

$$\mathcal{L} = \frac{1}{2}\left[\partial\phi\right]^2 - \frac{1}{2}m^2\phi^2 - \frac{\lambda}{24}\phi^4 \tag{1}$$

The theory has a $Z(2)$ symmetry, this breaks spontaneously if the thermal mass turns negative. By the choice of the bare mass parameter m we make sure that the system is deeply in the broken phase at zero temperature. The used quartic potential is motivated by the simple form of the classical kink solution:

$$\Phi(x, y) = v \tanh\left(Mx\right) \tag{2}$$

with

$$M^2 = -m^2/2 \quad \text{and} \quad v = \sqrt{-6m^2/\lambda}\,. \tag{3}$$

The tension of the wall is inversely proportional to the coupling: $\sigma = 4|m|^2/3\lambda$. In the classical limit the actual magnitude of the coupling is irrelevant as it can be scaled out. In the numerics we used $\lambda = 6M$. The only other parameter, the mass sets the scale for the evolution, we use the inverse wall width M to render all variables dimensionless, this numerically means $M = 1$.

We discretise the model on a spatial lattice. We solve a cut-off theory with a pre-set lattice spacing a. Since much of the physics of our interest is in the infrared, a plays little role. Based on earlier numerical experience we can use lattices as coarse as $aM = 0.5$. We repeated the presented numerical analysis on a coarser lattice ($aM = 0.7$) and found no significant difference. The lattice size L, however, matters. In order to avoid the interaction of a pair of signals originating from the same site we stop the simulation at $t = L/2$. This assumes that at $t = 0$ there is no correlation between any of the sites. Our initial condition will approximately satisfy this condition.

The initial condition can introduce other scales. We start the dynamics from a low energy density random configuration with a rich domain wall structure. Our main interest is how these walls evaporate under the realistic assumption that the scale in the initial condition separates from the microscopic scale M.

We designed the following numerical experiment. We start from a white noise configuration at $t = 0$, deep in the symmetric phase. We also checked the invariance of our results under replacing the initial noise by a (classical) thermal equilibrium of the same energy density. We then apply a cooling by adding a friction term to the kinetic term in the equation of motion: $\partial^2\phi \to \partial^2\phi + 2\gamma\partial_0\phi$. This evolution is non-physical, and we switch off at a conveniently chosen time when the particle content is negligible and the domain wall density reached a desirable value [53]. We starting the numerical observations only

after a short period of relaxation after the non-physical dynamics has been switched off. This corresponds to the pre-thermalisation time scale [43].

The field configuration at this instant is the initial condition of the dynamics of interest. We could set the origin of time to this instant, but we choose not to. The $t = 0$ point marks the onset of cooling, because at that point the correlation length is known to be of the microscopic scale.

B. Scaling solutions

The solution of classical dynamics is a straightforward computational task and being restricted to two spatial dimensions our resources allows for larger lattices ($L \geq 1000$), too.

As a first observation, we can estimate the domain wall length following the techniques detailed in Ref. [28], and reproduced their scaling solutions. In Fig. 1 we show the inverse domain wall density as a function of time. If the length scale (ℓ) of the domain wall network decouples from the microscopic scale, one may expect from dimensional reasons: $\ell^{-1} \sim Ł \sim t^{-1}$. The domain wall density Ł we define as the total length of domain walls on the lattice divided by the volume. A link on a lattice is considered as a part of a domain wall if the sites at its both ends have field amplitudes of opposite sign.

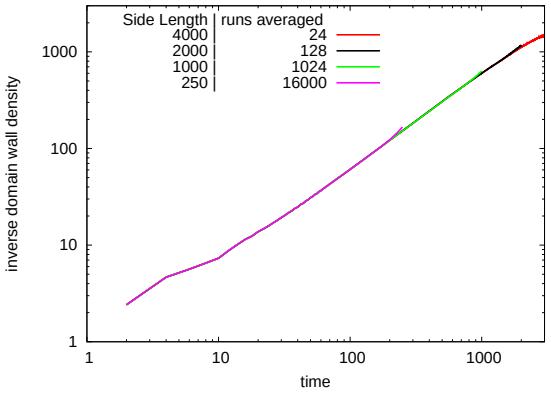

FIG. 1: Inverse domain wall density as a function of time. There is a perfect linear correspondence over at more than two orders of magnitude ($t = 10 \ldots 2000$), from the time of ending the damped evolution at $t = 10$ to the end of the simulation, when the walls' mean curvature radius is over 10^3 times larger than their width.

As always in classical field theory we always display an average over an ensemble of runs. (This is the thermal or white noise ensemble at $t = 0$. At positive times there is no randomness in the dynamics.) The averaged domain wall densities start deviating near $t \approx L$, slightly later than expected.

This scaling is a manifestation of a more generic feature in classical field theories, as it has been found in flat or curved space-time, and in two or three dimensions [28].

So that we gain more insight into the observed scaling we show a pair of lattice configurations in Fig. 2. The similarly looking snapshots were taken at times 50 and 100, respectively, but the earlier configuration we halved in linear size and scaled up accordingly. The time evolution appears to be equivalent to zooming.

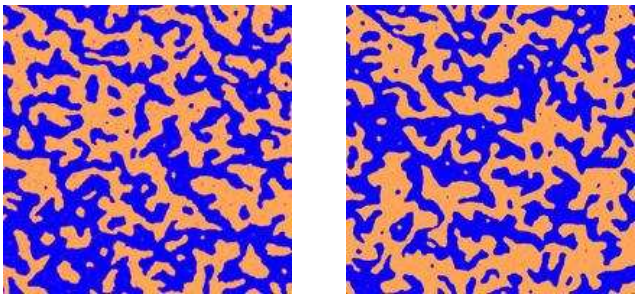

FIG. 2: Two snapshots of the lattice field configurations ($L = 2000$). Blue and orange regions show the domains of the degenerate vacua. To the left, we show the configuration at $t = 50$, we cropped the region $(0, L/2) \times (0, L/2)$ and scaled up by a factor of two. To the right we show the uncropped lattice at $t = 100$. There is no qualitative difference between the snapshots.

This feature can be made more formal in terms of the correlation function. We define our $C(r, t)$ correlation function as

$$C(r,t) = \frac{1}{L^2} \int dxdydz \, \langle \phi(x,z,t)\phi(y,z+r,t) \rangle \ , \qquad (4)$$

where $\langle \cdot \rangle$ denotes an ensemble averaging. If the more conventionally defined correlation function [54] $G(|\vec{x} - \vec{y}|, t) = \langle \phi(\vec{x}, t)\phi(\vec{y}, t) \rangle$ scales as $G(r, t) = t^{\alpha} G(r/t)$, it is easy to see that $C(r, t) = t^{\alpha+1} C(r/t)$. Indeed, Fig. 3 shows a numerical evidence for the scaling of C, with $\alpha \approx 0$. (If we require $t = 0$ to be the origin, the scaling law is only accurate to 10 %. If we fit the location of the origin of time and drop the initial evolution ($t < 200$), this we get an accuracy of 3%. The displacement of the origin fits to about -26).

III. HARTREE APPROXIMATION OF SCALAR FIELDS

In this section we review the inhomogeneous Hartree approximation and its application to our model. The reader can find a more detailed introduction in Ref. [39]. Its other name, Gaussian approximation, reflects the essence of the truncation of the dynamics: we disregard any connected higher n-point functions. Note in the context of the N-component scalar field the leading order in $1/N$ expansion leads to very similar (also Gaussian), but inequivalent approximation [44].

The operator equation in Heisenberg picture that we

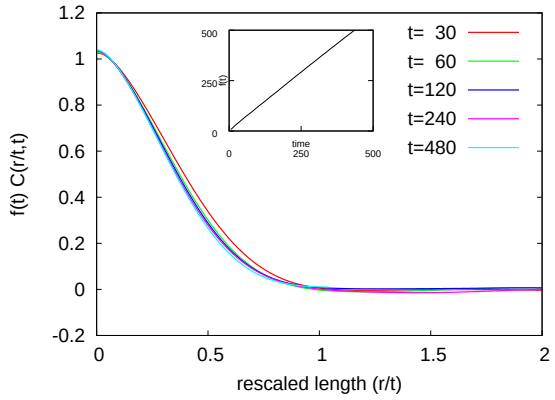

FIG. 3: Scaling of the equal time correlation function. Notice that the function has an approximate Gaussian shape, which is due to the nature of spinodal instability that created the domains. (There are deviations at small distance.) ($L = 1000$, 1024 runs averaged)

have to solve reads:

$$(\partial^2 + m^2)\hat{\phi}(\vec{x},t) + \frac{\lambda}{6}\hat{\phi}^3(\vec{x},t) = 0\,. \qquad (5)$$

We split off the quantum expectation value: $\hat{\phi}(\vec{x},t) = \bar{\Phi}(\vec{x},t) + \hat{\varphi}(\vec{x},t)$, with $\langle\hat{\varphi}(\vec{x},t)\rangle \equiv 0$.

The Hartree approximation basically means that we restrict the density operator of the $\hat{\varphi}$ degrees of freedom to Gaussian at all times. For such degrees of freedom $\hat{\varphi}_i$ we have the following identities: $\langle\hat{\varphi}_i^3\rangle = 0$ and $\langle\hat{\varphi}_i^3\hat{\varphi}_j\rangle = 3\langle\hat{\varphi}_i^2\rangle\langle\hat{\varphi}_i\hat{\varphi}_j\rangle$.

We can simply take the quantum average of Eq. (5), or multiply from the left by $\hat{\varphi}(\vec{y},t_y)$ and get an equation for the Wightman propagator $G^<(\vec{x},t_x;\vec{y},t_y) \equiv G^<(x,y)$ by averaging that, too:

$$\left[\partial_x^2 + m^2 + \frac{\lambda}{2}G^<(x,x)\right]\bar{\Phi}(x) + \frac{\lambda}{6}\bar{\Phi}^3(x) = 0\,, \qquad (6)$$

$$\left[\partial_x^2 + m^2 + \frac{\lambda}{2}\bar{\Phi}^2(x) + \frac{\lambda}{2}G^<(x,x)\right]G^<(x,y) = 0\,, \qquad (7)$$

It is remarkable that this simple truncation of the hierarchy of n-point functions leads to a self-consistent set of equations. Indeed, these are the Schwinger-Dyson equations for the propagator in the leading order truncation of the two-particle irreducible (2PI) effective action [45].

Gaussianity also implies that the Heisenberg operators at a finite time relate to the initial operators by a Bogolyubov transformation:

$$\hat{\varphi}(\vec{x},t) = \int\frac{d^dk}{(2\pi)^d}\left(\hat{a}_{\vec{k}}\psi_{\vec{k}}(\vec{x},t) + \hat{a}^+_{\vec{k}}\psi_{\vec{k}}{}^*(\vec{x},t)\right)\,. \qquad (8)$$

So that we have the text-book operator at $t = 0$ we set $\psi_{\vec{k}}(\vec{x},0) = e^{-i\vec{k}\vec{x}}/\sqrt{2\omega_k}$ and $\dot{\psi}_{\vec{k}}(\vec{x},0) = -i\omega_k\psi_{\vec{k}}(\vec{x},0)$. Here d is the number of space dimensions and $\omega_k^2 = \vec{k}^2 + m_r^2$, where m_r is the renormalized mass, often amended with a contribution from the background field. The ladder operators obey the usual $[\hat{a}_{\vec{k}_1},\hat{a}^+_{\vec{k}_2}] = (2\pi)^d\delta(\vec{k}_1 - \vec{k}_2)$ commutation relation. The initial particle spectrum are given by $\left\langle\hat{a}^+_{\vec{k}}\hat{a}_{\vec{k}}\right\rangle = n^0_{\vec{k}}$. These numbers appear in the equal time two-point function:

$$G^<(\vec{x},t,\vec{x},t) = \int\frac{d^dk}{(2\pi)^d}|\psi_{\vec{k}}(\vec{x},t)|^2(2n^0_{\vec{k}}+1) \qquad (9)$$

This obviously diverges even in two space dimensions. The initial infinite mass shift we compensate by a mass renormalisation and introduce the finite mass squared m_r^2 in the equation for $\psi_{\vec{k}}$:

$$\left[\partial_x^2 + m_r^2 + \frac{\lambda}{2}\bar{\Phi}(\vec{x},t)\right.$$
$$\left. + \frac{\lambda}{2}\int\frac{d^dk}{(2\pi)^d}\left[|\psi_{\vec{k}}(\vec{x},t)|^2 - \psi_{\vec{k}}(\vec{x},0)|^2\right](2n^0_{\vec{k}}+1)\right]\psi_{\vec{p}}(\vec{x},t) = 0 \qquad (10)$$

A coupling renormalisation is also necessary in three dimensions [46], but in this simple case we do not need to go beyond mass renormalisation.

The traditional way of solving the dynamics in Gaussian approximation involves Eqs. (6), (9) and (10). One normally discretizes the equations on a space lattice. A consistent Bogolyubov transformation requires that the $\vec{k}$ index of the mode functions runs in the entire Fourier space of the lattice. In addition to the trivial background equation on an N^2 lattice this means N^4 complex equations.

But mode function expansion is just one of the possible ways of solving Eqs. (6) and (7). Alternatively, we consider an ensemble of N_e classical trajectories $\varphi_i(\vec{x},t)$, solutions of the equation

$$\left(\partial_x^2 + m^2 + \frac{\lambda}{2}\left[\bar{\Phi}^2(\vec{x},t) + \left\langle\varphi^2(\vec{x},t)\right\rangle_E\right]\right)\varphi_i(\vec{x},t) = 0\,. \qquad (11)$$

Here $\langle\cdot\rangle_E$ stands for the ensemble average. Indeed, multiplying the equation with $\varphi_i(\vec{y},t_y)$ and averaging over i (ensemble average), will bring us back to Eq. (7) with $G^< \to G^e = \langle\varphi(\vec{x},t_x)\varphi(\vec{y},t_y)\rangle_E$. But there will be no exact equivalence between ensemble and quantum averages: the quantum two-point function $G^<$ is complex, G^e is real. Notice, however, that the imaginary part of $G^<$ entirely decouples in Eq. (7), since the equal time propagator is always real.

Of course, $\varphi_i(\vec{x},t)$ must be properly initialized to form a Gaussian ensemble of the correct standard deviation:

$$\begin{aligned}
\langle\varphi(\vec{x},0)\varphi(\vec{y},0)\rangle &= \hbar\int\frac{d^dk}{(2\pi)^d}e^{-i\vec{k}(\vec{x}-\vec{y})}\frac{1}{\omega_k}\left(n^0_{\vec{k}}+\frac{1}{2}\right)\,,\\
\langle\dot{\varphi}(\vec{x},0)\dot{\varphi}(\vec{y},0)\rangle &= \hbar\int\frac{d^dk}{(2\pi)^d}e^{-i\vec{k}(\vec{x}-\vec{y})}\omega_k\left(n^0_{\vec{k}}+\frac{1}{2}\right)\,,\\
\langle\varphi(\vec{x},0)\dot{\varphi}(\vec{y},0)\rangle &= 0\,. \qquad (12)
\end{aligned}$$

Technically, we initialize φ in momentum space by a random phase and amplitude at the $t = 0$ and $t = \delta t$ time slices.

We intentionally introduced the factor $\hbar$, as a control parameter for the fluctuation φ. This way we can tune strength of the back reaction of the quantum fluctuations to the background. In the classical theory it was possible to scale out λ, here rescaling the field with $1/\sqrt{\lambda}$ would also require to rescale $\hbar$ with λ. If we stick to $\lambda = 6M$ in the numerics, it is the $\hbar$ in Eq. (12) that one can use to vary the coupling, effectively.

Numerically, it is much simpler to solve $N_e N^2$ real equations than N^4 complex ones, we found that even an ensemble of $1 \ll N_e \ll N^2$ was big enough. The simple structure of Eq. (11) allows high speed implementations [55]. We note that the equation is not stable without manually fixing $\langle \varphi_i(\vec{x}) \rangle = 0$ after every leap-frog time step.

Before embarking into the analysis of numerical results, let us pause to discuss in what sense the Hartree equations represent a quantum correction to the classical dynamics.

Notice that we can arrive at Eqs. (6) and (7) also from a different concept. Let us start a number of classical trajectories from an initial Gaussian ensemble (e.g. Eq. (12)). Instead of following the individual trajectories we can write down the equations for the n-point functions. Simply discarding the three or higher order correlators we get a closed set of equations, that coincide with Eqs. (6) and (7). We would also arrive to the same equations by truncating the 2PI effective action for the classical (or quantum) field theory to leading order.

Indeed, whether we start from a classical or quantum Gaussian ensemble, the genuine quantum features start to appear if we keep the four-point equation at least. A self-consistent set of equations follows from the next-to-leading order truncation of the 2PI effective action, where one easily identifies the term, responsible for quantum effects [47].

This statement, however, means that to Hartree order it is only the initial condition that reflects quantum physics. Do the mode function equations (10) or the propagator equation (7) introduce quantum corrections at all?

The answer is yes. If we consider one single classical trajectory $\bar{\Phi}$, switching on $\hbar$ in Eqs. (12) will definitely enable many quantum phenomena, such as vacuum particle production. Instead of doing Hartree, one can, of course, consider an ensemble of $\bar{\Phi}$ fields, initialized (as usual) with the just-the-half rule (analogous to Eqs. 12) and evolve them classically. This classical ensemble will equally enable the same quantum phenomena, but it will bring in several classical artefacts, too, such as the decay of the quantum zero-point energy. These artefacts can most simply eliminated by shutting down all higher loop diagrams, down to the order where quantum and classical approximations agree: this is the Hartree approximation.

Although it is possible to properly include higher order corrections [32, 33], they are not inevitable in the following two extremes: If the particle numbers are low, the higher order quantum corrections, that account for scattering of the quantum fluctuations, are not very important compared to the dynamics of other energetic objects, such as defects. If the particle numbers are very high, higher order quantum corrections are crucial, but they can be well estimated by a classical ensemble, here $n_{\vec{k}}$ dominates in $n_{\vec{k}} + 1/2$ and the classical artefacts will then be suppressed.

In the application considered in this paper we work with low particle numbers produced by the sparse network of defects. We believe that we do not miss the magnitude of the particle's back-reaction by ignoring the thermalisation of their spectral distribution. This semi-classical approach, however, approximates the damping of the classical degree of freedom at the lowest order.

IV. CLASSICAL VERSUS HARTREE DYNAMICS

The initial conditions given in section II A define a (highly non-Gaussian) ensemble of domain wall configurations at $t = 15$. For each member $\bar{\Phi}_i$ we define a (Gaussian) sub-ensemble of fluctuations. We follow the dynamics of this sub-ensemble in the Hartree approximation. The final averaging over the domain wall configurations occurs at the very end of the calculation. At the time we switch on the quantum equations (11) we renormalize the mass and thereby allow a smooth transition to quantum evolution.

In Fig. 4 we show the evolution of the power spectrum of the background field. In classical field theory this is the only degree of freedom, whereas in the Hartree approximation energy may drift into the "modes" (the ensemble of quantum fluctuations).

The correlation length in Fig. 5 is defined by a Gaussian fit to the correlation function shown in Fig. 3. In harmony with Fig. 4 we see no impact of the quantum fluctuations on the evolution of the macroscopic degrees of freedom. If all the domain wall loops were macroscopic, this would suggest that inverse total length of domain walls shown in Fig. 5 receives no significant quantum correction. Indeed, we again find a linear scaling, and we could not find a significant correction to the slope parameter for $t > 150$. But the inverse domain wall density is not entirely linear. In the first half of the evolution it drifts away the classical solution. This reflects a transient decay of some classically more stable structures.

The power spectrum in Fig. 4 does not give account on the created particles. The power spectrum of the $\varphi_x(\vec{x}, t)$ functions in Eq. 11 reflect the created particles. This spectrum does not scale, and performs a "boring" evolution: only the amplitude changes slightly and always resembles the vacuum power spectrum. This confirms the assumption that the particles are created on the mass scale and not e.g. in the infrared. At and beyond the

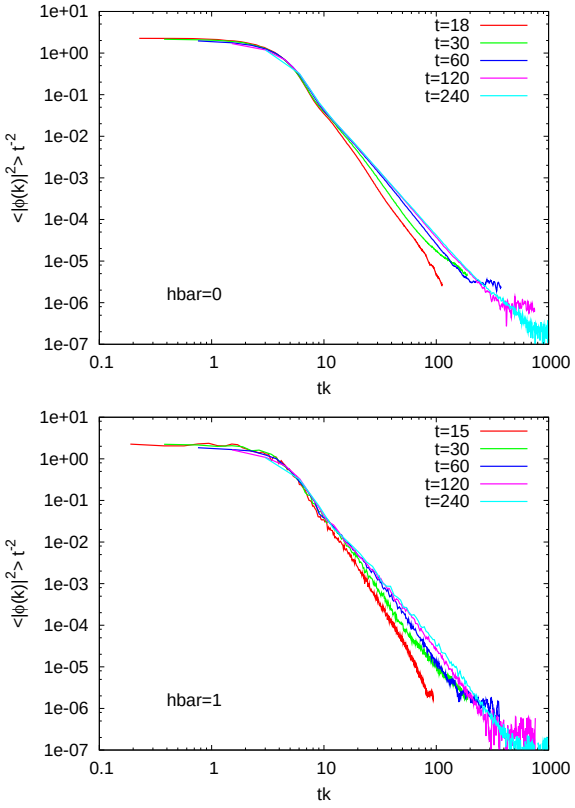

FIG. 4: The scaling of the power spectrum. The macroscopic part (domain walls) clearly follows the scaling law both in the classical (top) and in the quantum (bottom) case. The scaling breaks at the tail of the spectrum (small classical structures). ($L = 500$, average of 16000 and 192 runs for $\hbar = 0$ and 1, respectively.)

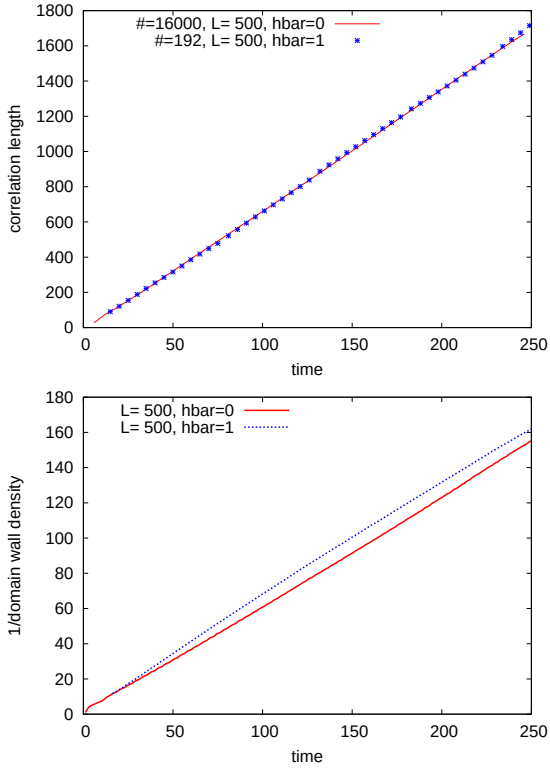

FIG. 5: The scaling of the correlation length (top) and the domain wall density (bottom)

mass scale the quantum fluctuations dominate over the classical structures in the power spectrum.

By construction of the initial conditions the energy density transferred from the domain walls to the fluctuations does not significantly raise the temperature and so the thermal mass. It was an important assumption in our analysis that the wall width M is constant in time.

The domain wall density and the correlation length are the key observables when we discuss scaling. Irrespectively to the coupling (λ) or the strength of the fluctuations ($\hbar$) we fit $\xi \approx 3.4(2) \cdot t$. For the domain wall density we find $\mathcal{L} = l/L^2 \approx 1.66(3)/t$ for our initial condition, where l is the total counted length of domain walls on the lattice at a given time. It is remarkable that these dimensionless coefficients are robustly insensitive to the variation of the coupling or the value of $\hbar$. Also it does not depend on the lattice spacing nor on the initial noise amplitude or the details of the cooling procedure.

To gain more insight into the small discrepancy between the quantum and classical domain wall density we count the number of domains, and use this number to estimate the loop number density ($n(t) = N(t)/L^2$). We applied a cluster algorithm on the lattice and plotted the resulting number density in Fig. 6. The effect of the quantum fluctuations is now striking.

In the approximated quantum theory we get what we think we should: if the correlation length $\xi \sim t$ scales linearly, any number density must scale as $n_q \sim t^{-2}$. The conclusion from Fig. 6 is that in the classical theory the domain number is dominated by microscopic structures. One hint for the smallness of these "mini-domains" is that the inverse wall width M must appear in the $n_{cl}(t) \sim M/t$ scaling rule for dimensional reasons, and its coefficient is not extreme. We can directly measure an average defect loop size by counting the loops (or domains, practically) that are in excess in the classical solution. The total wall length is also bigger in the classical case than with quantum correction. We used their quotient to estimate the size of these loops in Fig. 6. Unfortunately our numerics is not conclusive at later times, we expect this ratio to settle at a positive value $\sim M^{-1}$.

To find out more about these small classical structures let us compare the lattice snapshots taken from the same run with and without quantum fluctuations. We picked the time $t = 40$ and cropped a larger lattice appropriately so that we can show the most phenomena in one image: Fig. 7

In these images the black regions correspond to the $\bar{\Phi} > 0$ domains. We plotted the $\bar{\Phi} < 0$ domain with better colour resolution. The left hand side plot corresponds to the classical evolution, it shows many ripples and nu-

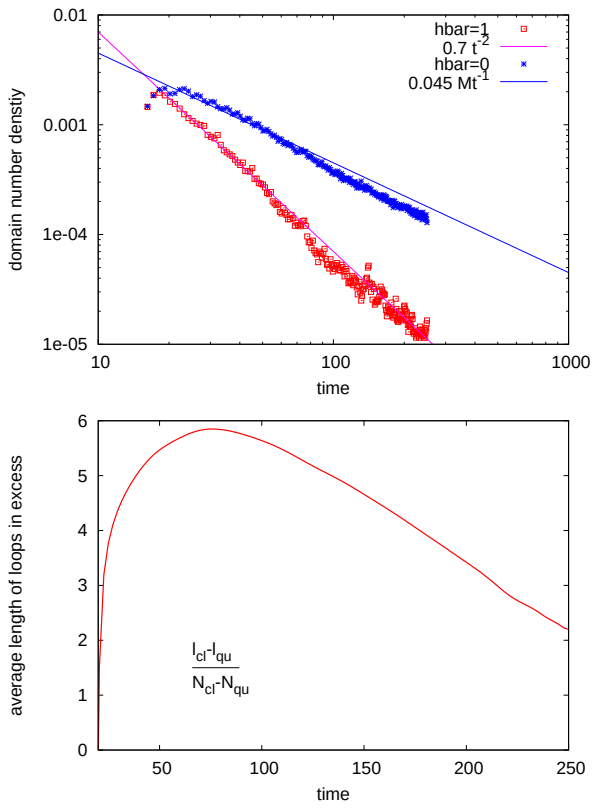

FIG. 6: Number of domains over lattice volume (top) in the classical and quantum framework. The classical scaling is counter intuitive. Dividing the difference of the total loop length by the number of loops (estimated by the number of domains) we get an average loop size (bottom).

merous dark spots where $\bar{\Phi}$ goes locally close or beyond zero. In the middle (quantum) plot we see fewer ripples and some (but not all) of the dark spots of the classical plot are missing here. To the right, we demonstrate the excitation of the quantum modes by plotting $\langle \varphi^2(\vec{x},t) \rangle_E$. These fluctuations are the strongest on the domain walls, which we interpret as particles in the bound state.

Looking at a sequence of such snapshots gives more detail about how these ripples are produced. As the domain walls shrink they emit classical waves, with a wave length of few times the wall width. These waves are equally present in the quantum case as well, where they are more damped. In the quantum fluctuation plot we also find traces of the classical ripples, but the spatial distribution of the produced particles appears to be smooth, and the ripples in $\langle \varphi^2(\vec{x},t) \rangle_E$ are an order of magnitude smaller than in $\bar{\Phi}^2$.

On the snapshots we marked the interesting places by letters. In both sides of the letter "A" the ripples are locally so high in amplitude that these spots are counted as a domain by the cluster algorithm and they contribute to the total length of domain walls. But they are not counted into the statistics of walls in the quantum case, since then their amplitude is within the threshold of zero field value. The amplitude of these spots actually oscillates, this is why we do not see the one on the right hand side of the letter "A" in the quantum plot. "B" marks the centre of ripples emitted earlier by the collapsing bubble marked with "D". These are mostly damped in the quantum run. The waves around the bubble "D" are higher in amplitude than in the quantum case. Finally, there is a spot with strongly oscillating amplitude, marked with "C". The magnitude of the quantum fluctuations oscillate coherently with the background field value.

V. DISCUSSION

Let us summarize the numerical findings: The correlation length, which is fitted from the correlation function in direct space, reflects the macroscopic evolution. We find that the known scaling behaviour is unperturbed by quantum effects. On the microscopic level, however, where the scaling is broken, we find stronger quantum effects, as expected.

We also find, that there are "mini-domains" in the classical simulation, that (at least partly) disappear if we switch on the quantum degrees of freedom. Its simplest explanation is that there are classically stable small structures that decay in a quantum field theory. Now we can speculate what these could be. Natural candidates are oscillons, localised oscillating wave packets, which are (quasi-)stable solutions of the classical field theory [48, 49].

If these small structures are indeed oscillons, their stability is enhanced by low dimensionality. If in three dimensions they are subject to a more rapid decay [50, 51], making the quantum decay channel less significant and hence the quantum correction to the scaling even smaller.

Indeed, a closer look on the lattice field revealed that there are small regions (with a diameter of O(5) domain wall width) that oscillate with a frequency $\sim M$. But oscillons are not the only structures that appear. The shrinking and collapsing domain walls emit classical waves with a wave length $\sim M^{-1}$. We see these waves on the lattice snapshots as circular ripples. These ripples from various sources interfere and at the points of constructive interference the field value may locally exceed zero and will then be counted as a small domain.

Classical waves are emitted in the quantum field theory, too. In quantum mechanics this classical excitation is known as coherent state, which transforms into an enlarged width of the wave function, or into particles in field theory language. This is the point where quantum corrections enter: the classical waves are damped and their interference results in fewer and less stable localised oscillating wave packets.

In this picture there is a non-perturbative classical mechanism that converts the energy stored in the string (or domain wall) to microscopic objects. In a field theory, these objects are neither loop fragments, nor particles, but coherent oscillations of the field expectation value.

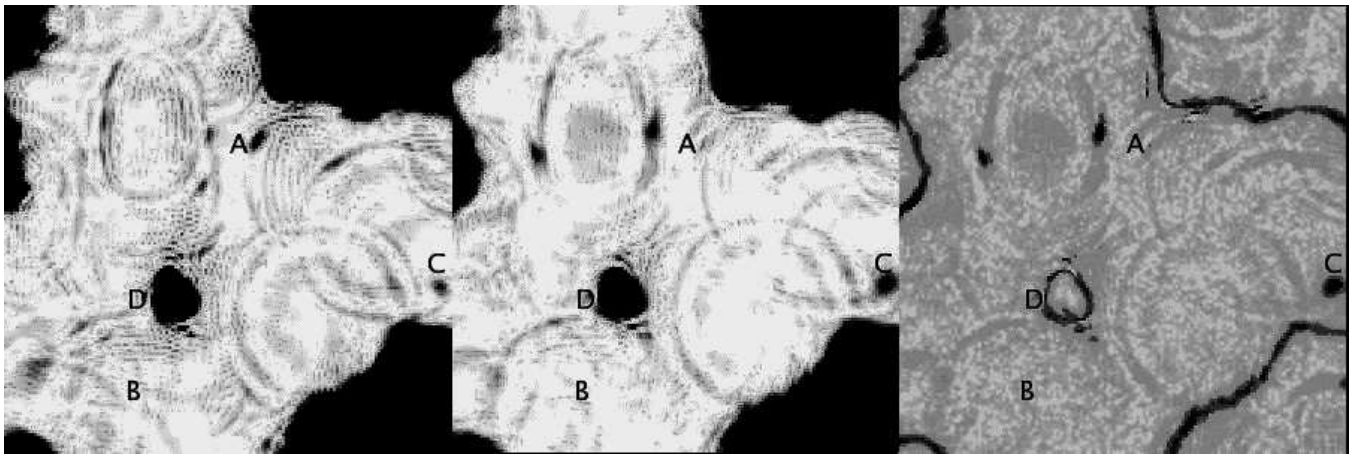

FIG. 7: Snapshot from a classical (left) and the corresponding quantum (middle) run. To the right the particle content is characterized by $\left\langle \varphi^2(\vec{x},t)\right\rangle_E$. The darker points mean higher value. (These images were taken at $t = 40$ on a $L = 128$ lattice. We cropped out a piece of 75×75)

Our numerics suggests that the scale of these classical waves are on the microscopic scale M. We observe that these waves are emitted from structures of size ℓ, presenting us with the challenge of explaining energy transport over a huge scale separation, $M\ell \sim 10^3$ at the end the simulation.

It is clear from the shown numerics that the domain wall decay was not enhanced by the quantum fluctuations and this conclusion we checked to stay true with $\hbar = 2$ or $\lambda = 12$. There is no indication for a direct decay channel into particles. A direct decay might also manifest in the sensitivity to the choice of the lattice spacing as we switched between $aM = 0.5$ and 0.7, but we found no significant difference. However, the decay of the classical waves and oscillons is no longer protected by scale separation.

Finally, let us attempt to understand Fig. 6. The energy density associated to macroscopic D-dimensional defects in d dimensions is $\sim M^{1+D}t^{D-d}$. Their decay releases energy at a rate of $\sim M^{1+D}t^{D-d-1}$. This energy is used to produce high amplitude classical structures (e.g. oscillons) that may have been counted as small domains. Since they emerge on the microscopic scale, their number density has a source of $C_{source}M^D t^{D-d-1}$, where C_{source} and the other constants we introduce here are dimensionless numbers of $\mathcal{O}(1)$. These small structures can decay in various ways: a) In the quantum calculation we include the direct quantum mechanical decay into particles with a rate of $\Gamma \sim M$; b) The small objects can be hit by a domain wall or string, its rate is proportional to the defect density: $C_{defect}M^{D-d+1}t^{D-d}$; c) These objects can also hit each other and annihilate. The probability of a given small object to meet an other one is proportional to its density n, which gives a rate of $C_{coll}M^{1-d}\,n$. These together give the following equation for the density n

$$\dot{n}+\Gamma n+C_{defect}\frac{M^{D-d+1}}{t^{d-D}}n+C_{coll}M^{1-d}n^2 = C_{source}\frac{M^D}{t^{d-D+1}} \tag{13}$$

If the quantum decay into particles dominates giving a finite life time to these small classical structures, the density n simply follows the source. Indeed we see $n \sim t^{-2}$ in Fig. 6. In the absence of Γ, however, we find that $n \sim M/t$ solves Eq. (13) in consistence with our observation. Since in this case n shows the same scaling as the domain wall density, counting them as defects does not spoil the observation of scaling. The classical approximation of Eq. (13) suggests that for $d > 2$ the collision term would dominate, giving $n \sim t^{-2}$. In higher dimensions, however, oscillons and other analogous structures are less stable, which introduces a decay term of classical nature bluring difference between classical and quantum scaling.

VI. CONCLUSION

In this paper we integrated the classical field equations as well as the Hartree approximated quantum evolution of a scalar field in the broken phase, starting from a network of domain walls. The scaling of macroscopic observables was manifest also in the quantum theory. Our numerical results suggest that the direct decay of domain walls into particles is insignificant, as the perturbative estimates predict. We can instead attribute the decay to the emergence of classical waves and other structures, such as oscillons. Since these coherent excitations of the quantum field theory are produced at the microscopic scale, their perturbative decay is no longer suppressed by the separation of scales. The production of large-amplitude classical oscillations is a genuine non-perturbative phenomenon that deserves further investi-

gation, as a similar effect is seen to drive the decay of cosmic strings in three dimensional field theory simulations [22]. Understanding the dominant decay channel of strings is of crucial importance for computing their observational signals.

Acknowledgments

The authors thank Jürgen Berges and Anders Tranberg for the encouraging discussions and also acknowledge the collaboration with Petja Salmi on a related project. The numerical work has been carried out on the Archimedes cluster of the University of Sussex. SB is funded by STFC.

[1] T. W. B. Kibble, J. Phys. A **9**, 1387 (1976).
[2] A. Vilenkin and Q. Shafi, Phys. Rev. Lett. **51**, 1716 (1983).
[3] M. B. Hindmarsh and T. W. B. Kibble, Rept. Prog. Phys. **58** (1995) 477
[4] A. Vilenkin and E.P.S. Shellard, "Cosmic Strings and Other Topological Defects," (Cambridge Univ. Press, Cambridge, 1994).
[5] N. Bevis, M. Hindmarsh, M. Kunz and J. Urrestilla, Phys. Rev. D **75**, 065015 (2007) N. Bevis, M. Hindmarsh, M. Kunz and J. Urrestilla, Phys. Rev. Lett., to appear [arXiv:astro-ph/0702223]; N. Bevis, M. Hindmarsh, M. Kunz and J. Urrestilla, Phys. Rev. D **76**, 043005 (2007) J. Urrestilla, N. Bevis, M. Hindmarsh, M. Kunz and A. R. Liddle, arXiv:0711.1842 [astro-ph].
[6] P. Goddard, J. Goldstone, C. Rebbi and C. B. Thorn, Nucl. Phys. B **56** (1973) 109.
[7] M. Srednicki and S. Theisen, Phys. Lett. B **189** (1987) 397.
[8] R. H. Brandenberger, Nucl. Phys. B **293** (1987) 812.
[9] N. Turok, Nucl. Phys. B **242**, 520 (1984). T. Vachaspati and A. Vilenkin, Phys. Rev. D **31** (1985) 3052. C. J. Burden, Phys. Lett. B **164**, 277 (1985).
[10] A. Albrecht and N. Turok, Phys. Rev. D **40**, 973 (1989). A. Albrecht and N. Turok, Phys. Rev. Lett. **54**, 1868 (1985).
[11] D. P. Bennett and F. R. Bouchet, Phys. Rev. Lett. **60**, 257 (1988).
[12] B. Allen and E. P. S. Shellard, Phys. Rev. Lett. **64**, 119 (1990).
[13] T. W. B. Kibble, Nucl. Phys. B **252** (1985) 227 [Erratum-ibid. B **261** (1985) 750].
[14] A. G. Smith and A. Vilenkin, Phys. Rev. D **36**, 990 (1987).
[15] M. Sakellariadou and A. Vilenkin, Phys. Rev. D **42**, 349 (1990).
[16] G. R. Vincent, M. Hindmarsh and M. Sakellariadou, Phys. Rev. D **56**, 637 (1997)
[17] C. Ringeval, M. Sakellariadou and F. Bouchet, JCAP **0702**, 023 (2007)
[18] C. J. A. Martins and E. P. S. Shellard, Phys. Rev. D **73**, 043515 (2006)
[19] K. D. Olum and V. Vanchurin, Phys. Rev. D **75**, 063521 (2007)
[20] G. N. Felder, J. Garcia-Bellido, P. B. Greene, L. Kofman, A. D. Linde and I. Tkachev, Phys. Rev. Lett. **87** (2001) 011601
[21] L. Kofman, A. D. Linde and A. A. Starobinsky, Phys. Rev. Lett. **76**, 1011 (1996)
[22] G. Vincent, N. D. Antunes and M. Hindmarsh, Phys. Rev. Lett. **80** (1998) 2277
[23] J. N. Moore, E. P. S. Shellard and C. J. A. Martins, Phys. Rev. D **65**, 023503 (2002)
[24] M. Yamaguchi, Phys. Rev. D **60**, 103511 (1999) M. Yamaguchi, J. Yokoyama and M. Kawasaki, Phys. Rev. D **61**, 061301 (2000)
[25] M. Hindmarsh and P. M. Saffin, JHEP **0608**, 066 (2006)
[26] A. Achucarro, P. Salmi and J. Urrestilla, Phys. Rev. D **75**, 121703 (2007)
[27] J. Urrestilla, N. Bevis, M. Hindmarsh, M. Kunz and A. R. Liddle, arXiv:0711.1842 [astro-ph].
[28] T. Garagounis and M. Hindmarsh, Phys. Rev. D **68**, 103506 (2003)
[29] J. C. R. Oliveira, C. J. A. Martins and P. P. Avelino, Phys. Rev. D **71**, 083509 (2005)
[30] P. P. Avelino, C. J. A. Martins, J. Menezes, R. Menezes and J. C. R. Oliveira, Phys. Lett. B **647**, 63 (2007)
[31] J. Berges AIP Conf. Proc. **739**, 3 (2005)
[32] J. Berges and J. Serreau, Phys. Rev. Lett. **91**, 111601 (2003)
[33] J. Berges, Nucl. Phys. A **699**, 847 (2002)
[34] A. Rajantie and A. Tranberg, JHEP **0611** (2006) 020
[35] F. Cooper and E. Mottola, Phys. Rev. D **36** (1987) 3114.
[36] D. Boyanovsky and H. J. de Vega, Phys. Rev. D **47** (1993) 2343; F. J. Cao and H. J. de Vega, Phys. Rev. D **65** (2002) 045012
[37] S. Y. Khlebnikov and I. I. Tkachev, Phys. Rev. Lett. **79** (1997) 1607
[38] J. Garcia-Bellido and A. D. Linde, Phys. Rev. D **57**, 6075 (1998)
[39] M. Salle, J. Smit and J. C. Vink, Phys. Rev. D **64** (2001) 025016
[40] M. Salle, J. Smit and J. C. Vink, Published in "Marseille 2000, Strong and electroweak matter" 321-326 arXiv:hep-ph/0009120. M. Salle, J. Smit and J. C. Vink, Nucl. Phys. B **625** (2002) 495
[41] L. M. Bettencourt, K. Pao and J. G. Sanderson, Phys. Rev. D **65** (2002) 025015
[42] M. Salle, Phys. Rev. D **69** (2004) 025005
[43] J. Berges, S. Borsanyi and C. Wetterich, Phys. Rev. Lett. **93** (2004) 142002
[44] B. Mihaila, T. Athan, F. Cooper, J. Dawson and S. Habib, Phys. Rev. D **62** (2000) 125015
[45] J. M. Cornwall, R. Jackiw and E. Tomboulis, Phys. Rev.

D **10** (1974) 2428.
[46] J. Baacke, K. Heitmann and C. Pätzold, Phys. Rev. D **55** (1997) 2320
[47] G. Aarts and J. Berges, Phys. Rev. Lett. **88** (2002) 041603
[48] E. J. Copeland, M. Gleiser and H. R. Muller, Phys. Rev. D **52** (1995) 1920
[49] M. Hindmarsh and P. Salmi, Phys. Rev. D **74**, 105005 (2006) M. Hindmarsh and P. Salmi, in preparation.
[50] G. Fodor, P. Forgacs, P. Grandclement and I. Racz, Phys. Rev. D **74**, 124003 (2006)
[51] P. M. Saffin and A. Tranberg, JHEP **0701**, 030 (2007)
[52] It should be noted that there is apparent disagreement between the three sets of authors on the interpretation of their results. We base our assertion on the observation that the peaks of the loop production function and the loop distribution function remain near the initial correlation length.
[53] We typically used a cooling of $\gamma = 0.5$ in the range $t = 0 \ldots 10$, followed by a relaxation period of 5 units. The initial energy density before cooling was set to 2.3.
[54] We prefer to use C in the numerics for its simplicity and also because it is the Fourier transform of the power spectrum. It simply relates to G if we assume isotropy and large volume. We only show data for times where these conditions are granted.
[55] Two of the important optimizations: we use the single precision SSE extension of the i386 architecture and that we loaded $\varphi_i(\vec{x}, t)$ into the cache once in a time step, only.